

Quantum entanglement of fermionic symmetry-enriched quantum critical points in one dimension

Wen-Hao Zhong,^{1,2} Hai-Qing Lin,² and Xue-Jia Yu^{1,3,*}

¹*Department of Physics, Fuzhou University, Fuzhou 350116, Fujian, China*

²*Institute for Advanced Study in Physics and School of Physics, Zhejiang University, Hangzhou 310058, China*

³*Fujian Key Laboratory of Quantum Information and Quantum Optics,*

College of Physics and Information Engineering, Fuzhou University, Fuzhou, Fujian 350108, China

(Dated: August 19, 2025)

Quantum entanglement can be an effective diagnostic tool for probing topological phases protected by global symmetries. Recently, the notion of nontrivial topology in critical systems has been proposed and is attracting growing attention. In this work, as a concrete example, we explore the quantum entanglement properties of fermionic symmetry-enriched quantum critical points by constructing exactly solvable models based on stacked multiple Kitaev chains. We first analytically establish the global phase diagram using entanglement entropy and reveal three topologically distinct gapped phases with different winding numbers, along with three topologically distinct transition lines separating them. Importantly, we unambiguously demonstrate that two transition lines exhibit fundamentally different topological properties despite sharing the same central charge. Specifically, they display nontrivial topological degeneracy in the entanglement spectrum under periodic boundary conditions, thereby generalizing the Li-Haldane bulk-boundary correspondence to a broader class of fermionic symmetry-enriched criticality. Additionally, we identify a novel Lifshitz multicritical point at the intersection of the three transition lines, which also exhibits nontrivial topological degeneracy. This work provides a valuable reference for investigating gapless topological phases of matter from the perspective of quantum entanglement.

I. INTRODUCTION

Topological phases of matter form a cornerstone in modern condensed matter physics and quantum information science, extending beyond the traditional Landau-Ginzburg symmetry-breaking paradigm [1–4]. To date, most well-understood topological phases have focused on gapped quantum systems, ranging from symmetry-protected topological (SPT) phases, which include both free fermions [5–8] and strongly correlated many-body systems [9–12], to intrinsically topologically ordered phases features by fractionalized anyonic excitations [13–18]. However, recent advances suggest that symmetry-protected topology can persist even in gapless systems, including continuous quantum critical points (QCPs) and stable critical phases, collectively referred to as gapless symmetry-protected topological (gSPT) phases [19–56]. Among these, nontrivial topology in free fermion critical systems have attracted particular attention due to their exact solvability [30, 52, 57], making them valuable for establishing a general theory of fermionic symmetry-enriched QCPs in arbitrary dimensions. In contrast, higher-dimensional interacting critical systems remain challenging due to the lack of efficient analytical and numerical tools.

A central task is to classify and characterize topological phases in a unified framework. Traditionally, gapped topological phases are considered to share the same bulk properties as trivial quantum paramagnets, exhibiting topological distinctions only when open boundaries are present [3, 9–11]. Similarly, in the case of symmetry-enriched QCPs, the bulk universality class of topological gapless systems is identical to their trivial counterparts, while symmetry-protected edge modes emerge under open boundary conditions [29, 32]. As a

result, these topological phases cannot be detected using local observables in the bulk. However, previous studies [12, 33, 58–70] suggest that quantum entanglement serves as a definitive signature of both topological and critical phases, with entanglement entropy and the entanglement spectrum being the most representative physical quantities. The former captures universal data, such as the central charge, in the conformal critical points within certain universality classes [71, 72], while the latter encodes nontrivial topological degeneracy and acts as a fingerprint for identifying topological phases [33, 59, 61]. Specifically, the entanglement spectrum under periodic boundary conditions, known as the bulk entanglement spectrum, encodes the topological degeneracy of the energy spectrum under open boundary conditions, which is referred to as the Li-Haldane conjecture [59], has recently been generalized to bosonic symmetry-enriched QCPs in quantum spin chains [33, 50]. Therefore, the bulk entanglement spectrum provides an effective diagnostic probe that does not require boundaries and preserves all symmetries of the system, including lattice symmetries.

A promising direction is to use the information-theoretic concept of entanglement to characterize free fermionic symmetry-enriched QCPs, which allows us to be analytically tractable and avoids the computational challenges associated with gapless many-body systems. Consequently, similar to the extensively studied quantum entanglement properties of free-fermion topological insulators and superconductors [60, 63–65, 73], we can explore analogous questions for free-fermion symmetry-enriched critical states: What are the quantum entanglement properties of these states? More importantly, can we uncover novel entanglement signatures at the transition points between these fermionic symmetry-enriched QCPs?

In this work, we address the series of questions outlined above using an exactly solvable Majorana fermion model, constructed by stacking multiple Kitaev chains. Using entanglement entropy as a diagnostic, we analytically establish the

* xuejiayu@fzu.edu.cn

global phase diagram, which exhibits three types of gapped phases characterized by distinct topological winding numbers ($\omega = 0, 1, 2$). The three conformal critical lines, which separate the topologically distinct gapped phases, can be determined analytically, while a nonconformal Lifshitz multicritical point emerges at the intersection of these transition lines. Through finite-size scaling analysis of entanglement entropy, we find that both transitions between the $\omega = 1$ topological superconducting (TSC) phase and either the trivial or the $\omega = 2$ TSC phase belong to the Majorana universality class with central charge $c = 1/2$. In contrast, the transition between the trivial and the $\omega = 2$ TSC phase belongs to the Dirac universality class with $c = 1$. Furthermore, we employ the bulk entanglement spectrum as a probe to characterize the nontrivial topology of these quantum critical lines. Our numerical results unambiguously demonstrate that only the transition lines between TSC phases with different winding numbers exhibit topological degeneracy in the entanglement spectrum, corresponding to fermionic symmetry-enriched QCP. In contrast, the remaining two transition lines are both topologically trivial, even though one of them shares the same central charge ($c = 1/2$) as the topologically nontrivial one. Finally, we explore the topological properties at the Lifshitz multicritical point by examining its bulk entanglement spectrum, revealing a topological Lifshitz multicritical point with nontrivial degeneracy.

The paper is organized as follows: Section. II introduces the physics of the Majorana α chain and presents the exactly solvable lattice model we focus on. Section. III (a) provides a self-contained review of entanglement entropy and spectrum, along with the calculation scheme for free fermion systems. Section. III (b) maps out the global phase diagram of the model using entanglement entropy. As a warm-up, we first examine the entanglement spectrum to identify different gapped topological phases in Section. III (c), and characterize critical and topological properties at three transition lines and the multicritical point in Section. III (d). The conclusions are presented in Section. IV, and additional data from our analytical and numerical calculations are provided in the Appendix.

II. MODEL: MAJORANA α CHAIN

The simplest model that exhibits both gapped SPT and symmetry-enriched QCPs is constructed by stacking α Kitaev chains on top of each other, which is equivalent to coupling Majorana modes over a distance $\alpha \in \mathbb{Z}$. This model, known as the Majorana α chain (abbreviated as α chain) [57, 74, 75], is described by the Hamiltonian:

$$H_\alpha = i \sum_n \tilde{\gamma}_n \gamma_{n+\alpha}, \quad \alpha \in \mathbb{Z}, \quad (1)$$

where the Majorana operators are expressed in terms of complex fermion operators c as $\gamma_n = c_n^\dagger + c_n$ and $\tilde{\gamma}_n = i(c_n^\dagger - c_n)$. Each unit cell consists of two Majorana fermions, γ_n (red) and $\tilde{\gamma}_n$ (blue), as illustrated in Fig. 1. The α -chain preserves both particle-hole C and time-reversal symmetry \mathcal{T} , which satisfy $\mathcal{T}^2 = C^2 = +1$. Consequently, the model belongs to the BDI

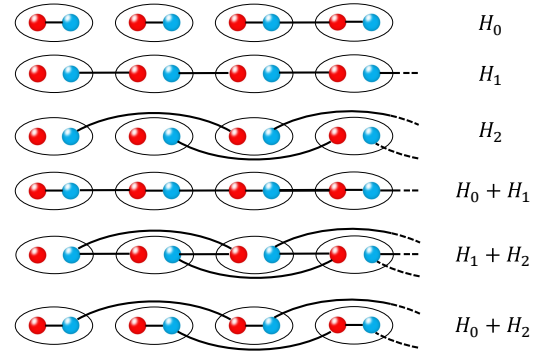


FIG. 1. (Color Online) The representative Hamiltonian of the Majorana α chain for both gapped and gapless phases is shown. Fermionic chains with $L = 4$ unit cells are depicted, where each unit cell consists of two sublattice sites, represented by red and blue circles. The unpaired Majorana fermions at the edges illustrate the topological nature of both the gapped and gapless states.

symmetry class [76]. As a result, the topological nature of α chains can be characterized by a discrete topological winding number $\omega = 0, 1, 2, \dots$. Moreover, linear combinations of different α chains can give rise to topologically distinct Majorana conformal field theory (CFT), leading to the concept of fermionic symmetry-enriched QCPs [35, 57]. Additionally, a nonconformal tricritical point emerges at the transition between these topologically distinct conformal critical lines.

Intuitively, the terms in H_α serve as fermionic duals of Ising spin Hamiltonians. For example, H_0 corresponds to the transverse field σ_n^x , representing a trivial band insulator. H_1 describes the Ising spin-spin interaction $\sigma_n^z \sigma_{n+1}^z$, while H_2 represents a cluster interaction $\sigma_n^z \sigma_{n+1}^x \sigma_{n+2}^z$, whose ground state belongs to a gapped cluster SPT phase [77–80].

Moreover, the composite Hamiltonians $H_0 + H_1$ and $H_1 + H_2$ correspond to topologically distinct critical Majorana chains, which are the fermionic duals of the critical transverse and cluster Ising models. These two critical points are both characterized by the same Ising CFT but exhibit distinct topological properties, such as degenerate edge modes even at criticality. This phenomenon is referred to as symmetry-enriched quantum criticality [29]. Under the Jordan-Wigner duality, these nontrivial topological critical points can also emerge in free fermion systems, giving rise to the fermionic symmetry-enriched QCPs.

We would like to emphasize that several important subtleties remain between symmetry-enriched quantum critical points in free fermion systems and those in interacting spin chains, which are elaborated upon below: i) The emergence of topological edge states in critical free fermion systems arises from a novel mechanism known as kinetic inversion, which is fundamentally distinct from the symmetry-enriched CFT framework used for interacting spin chains. Crucially, this mechanism does *not* rely on conformal symmetry, which is essential in the symmetry-enriched CFT description. ii) In interacting critical spin chains, the spatial decay of topological edge states can exhibit algebraic localization—an exotic feature that does not occur in free fermionic systems, where

edge states remain exponentially localized. iii) The exactly solvable nature of free fermion systems provides a valuable avenue for exploring gapless topology in higher dimensions, offering a platform that is tractable both analytically and numerically. More importantly, for free fermionic tight-binding models, the winding number—which is widely used to classify gapped topological insulators—is ill-defined in the gapless regime and cannot be directly generalized. As a result, the classification of gapless topological phases in free fermion systems remains an open question, particularly in higher dimensions, despite recent progress [29, 30, 57]. In contrast, the entanglement spectrum—the central diagnostic used in our work—can unambiguously distinguish between topologically trivial and nontrivial critical points, both in free fermion systems and in interacting critical spin chains [33]. Therefore, it serves as a robust and unique fingerprint for classifying topologically nontrivial critical points in gapless free fermion systems for arbitrary dimensions. A systematic exploration of the entanglement spectrum in gapless topological states of free fermion systems in general dimensions will be presented in our upcoming work.

In this work, to systematically investigate the entanglement properties of fermionic symmetry-enriched QCPs, we focus on the simplest exactly solvable Hamiltonian that incorporates a linear combination of α -chains, given by $H = g_0 H_0 - g_1 H_1 + g_2 H_2$, where, without loss of generality, we set $g_0 = 1.0$ as the energy unit. To understand the underlying quantum phases of this model, let us first consider the limiting cases: 1) When H_0 dominates, the ground state is a trivial product state. 2) When H_1 dominates, the system realizes a topological superconducting phase with a winding number $\omega = 1$, which is the fermionic dual of an Ising spontaneous symmetry breaking (SSB) phase with two-fold ground-state degeneracy. 3) When H_2 dominates, the system remains in a topological superconducting phase but with a winding number $\omega = 2$. The competition among H_0 , H_1 , and H_2 gives rise to a rich global phase diagram with intricate quantum entanglement properties, which are the central focus of this work.

III. RESULTS

A. Quantum entanglement of free fermion systems

To explore the quantum entanglement properties of fermionic symmetry-enriched QCPs, we first introduce the fundamental concepts of entanglement entropy and entanglement spectrum and then provide numerical details on how to compute these quantities in free fermion systems.

In quantum many-body systems, entanglement entropy serves as a key indicator of phase transitions by extracting relevant information from the ground-state wavefunction $|\varphi_0\rangle$. Typically, it is defined by partitioning the system into two subsystems, A and B, and computing the reduced density matrix for subsystem A by tracing out the degrees of freedom of subsystem B:

$$\rho_A = \text{Tr}_B(|\varphi_0\rangle\langle\varphi_0|). \quad (2)$$

The entanglement entropy, measuring the entanglement between parts A and B, is then expressed as:

$$S_A = -\text{Tr}[\rho_A \ln(\rho_A)]. \quad (3)$$

which is evaluated in terms of the eigenvalues of ρ_A . For a one-dimensional local quantum system with periodic boundary conditions, CFT suggests that the entanglement entropy for subsystem A with size l follows the finite-size scaling behavior [71, 72]

$$S_l \sim \frac{c}{3} \ln \left[\frac{N}{\pi} \sin \left(\frac{\pi l}{N} \right) \right] + S', \quad (4)$$

where c is the central charge, which varies for different universality classes, and S' is a non-universal constant. For half chain entanglement entropy $S_{l=N/2}$, the finite-size scaling relation reduced to $S(N) \sim \frac{c}{3} \ln N + S_0$. Another important entanglement-related quantity, known as the entanglement spectrum, consists of the eigenvalues of the modular or entanglement Hamiltonian H_A , which is related to the reduced density matrix ρ_A of the subsystem A by $\rho_A = e^{-H_A}$. These two fundamental entanglement measures—entanglement entropy and entanglement spectrum—serve as powerful tools for diagnosing both critical and topological properties in quantum many-body systems.

Calculating these two entanglement quantities is generally challenging. However, in free fermion systems, entanglement-based quantities can be computed analytically using the correlation matrix technique, which we briefly review below. For the ground state $|\Phi\rangle$ of free fermion system with half-filling, the total density matrix can be expressed in terms of correlation matrix [81–87]:

$$\rho = |\Phi\rangle\langle\Phi| = \det(I - \mathcal{G}) \exp \left(\sum_{ij} [\ln \mathcal{G}(I - \mathcal{G})^{-1}]_{ij} \Psi_i^\dagger \Psi_j \right), \quad (5)$$

where $\{\Psi_i\}$ is the Nambu basis which defined as $\Psi = (c_1, c_2, \dots, c_N, c_1^\dagger, c_2^\dagger, \dots, c_N^\dagger)^T$, and \mathcal{G} is the correlation matrix, given by

$$\mathcal{G}_{ij} = \begin{pmatrix} \langle c_i^\dagger c_j \rangle & \langle c_i^\dagger c_j^\dagger \rangle \\ \langle c_i c_j \rangle & \langle c_i c_j^\dagger \rangle \end{pmatrix} = \begin{pmatrix} C_{ij} & F_{ij} \\ F_{ji}^* & \delta_{ij} - C_{ji} \end{pmatrix}, \quad (6)$$

where C and F denote the normal and anomalous correlation matrix, respectively. To obtain the reduced density matrix ρ_A , we can restrict the correlation matrix to subsystem A to obtain the block correlation matrix $G = \mathcal{G}|_A$. Consequently, the reduced density matrix of subsystem A is given by

$$\rho_A = \det(I - G) \exp \left(\sum_{ij \in A} [\ln G(I - G)^{-1}]_{ij} \Psi_i^\dagger \Psi_j \right), \quad (7)$$

where indices i and j belong only to subsystem A. By diagonalizing the block correlation matrix G , we obtain

$$\rho_A = \exp \left(\sum_k \ln(1 - \xi_k) + \sum_n [\ln \xi_n(1 - \xi_n)^{-1}] \psi_n^\dagger \psi_n \right), \quad (8)$$

where $\{\psi_n\}$ is a new basis obtained from $\{\Psi_n\}$ via an Bogoliubov transformation, and $\{\xi_n\}$ are the eigenvalues of block correlation matrix G , which are directly related to the entanglement spectrum [83, 86, 87]. After this diagonalization, the reduced density matrix takes a diagonal form.

Thus, the entanglement entropy can be expressed in terms of the eigenvalues of the correlation matrix $\{\xi_n\}$:

$$S_A = - \sum_n [\xi_n \ln \xi_n + (1 - \xi_n) \ln(1 - \xi_n)]. \quad (9)$$

It is important to note that, due to particle-hole symmetry, the eigenvalues $\{\xi_n\}$ appear in pairs of the form $\{\xi_n, 1 - \xi_n\}$. As a result, when summing over the eigenvalues in Eq. (9), they should first be arranged in ascending order, and the summation should be performed over only the first half of the spectrum.

B. Global phase diagram from quantum entanglement

Before delving into the details of the numerical results, let us first summarize the global quantum phase diagram of the model in Eq. (1) from the entanglement perspective. The tuning parameters (g_1, g_2) drive the system into different phases, including both topologically trivial and nontrivial phases characterized by different winding numbers, as illustrated in Fig. 2. The ground states of the fixed-point Hamiltonians H_α with $\alpha = 0, 1, 2$ correspond to a trivial phase ($\alpha = 0$) and TSC phases with winding numbers $\omega = 1$ ($\alpha = 1$) and 2 ($\alpha = 2$), respectively. Away from the fixed-point limit, where competing interactions among g_0, g_1 , and g_2 are present, these three topologically distinct phases extend over finite regions of the phase diagram, which is further confirmed by the entanglement entropy within each phase, as shown in the color plot in Fig. 2. Specifically, we observe that within the phase regions, the entanglement entropy increases with the winding number. This is because a larger winding number indicates a larger number of fermionic edge modes under open boundary conditions, thereby contributing more entanglement in the TSC phases compared to the trivial phase.

Moreover, three phase transitions exist between these topologically distinct quantum phases, as evidenced by the numerical results of entanglement entropy shown in Appendix C. The transition points between the trivial and TSC phases, as well as between TSC phases with different winding numbers, exhibit topologically distinct Dirac cones [30, 88]. Specifically, all the transition lines in the phase diagram can be analytically derived—see Appendix A for details.

In summary, several key observations regarding the phase diagram are as follows:

- i) The conformal critical lines ($g_1 = g_2 + 1, 0 < g_2 < 1$) separating the trivial and $\omega = 1$ TSC phases belong to the topologically trivial Majorana universality class with central charge $c = 1/2$.
- ii) The conformal critical lines ($g_1 = g_2 + 1, g_2 > 1$) between the $\omega = 1$ and $\omega = 2$ TSC phases also belong to the $c = 1/2$ Majorana universality class but feature topologically protected edge modes under open boundary conditions. This class is now known as topological Majorana CFT.

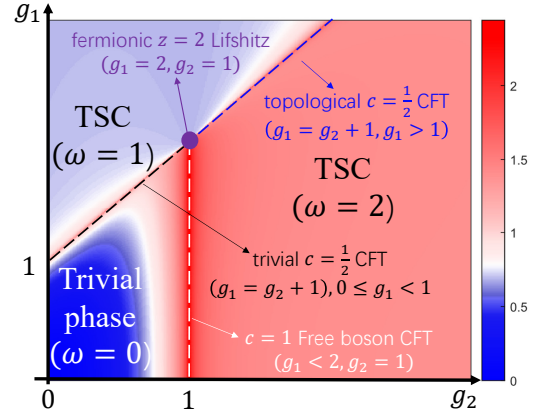


FIG. 2. (Color Online) The global phase diagram of $H = H_0 - g_1 H_1 + g_2 H_2$ is shown as a function of the two control parameters g_1 and g_2 . The TSC phases represent topological superconducting phases characterized by the winding number ω . The exact expressions for the three phase boundaries (depicted as dashed lines) can be determined analytically; see Appendix A for details. These transition lines are conformally invariant and exhibit distinct topological properties. The multicritical point (purple circle) is the only nonconformal critical point, described by the fermionic Lifshitz theory with a dynamical critical exponent $z = 2$, known as the fermionic Lifshitz multicritical point. The colorbar indicates the value of the entanglement entropy. Simulations are performed with a system size of $N = 400$.

iii) The conformal critical lines ($g_1 = 1, 0 < g_2 < 2$) separating the trivial and $\omega = 2$ TSC phases belong to the Dirac universality class with central charge $c = 1$.

iv) These three conformal critical lines intersect at a nonconformal multicritical point ($g_1 = 2, g_2 = 1$) with a dynamical exponent $z = 2$, known as the fermionic Lifshitz multicritical point.

A systematic investigation of the entanglement properties of these nontrivial critical states is the primary focus of this paper, which we will gradually reveal in the following sections.

C. Entanglement spectrum in gapped fermionic topological phase

The nontrivial topological degeneracy can be encoded in the bulk wavefunction without requiring any boundaries. A well-known principle of bulk-boundary correspondence is the Li-Haldane conjecture [59], which states that the low-lying entanglement spectrum of a bulk wavefunction can be exactly reconstructed from the energy spectrum under open boundary conditions. This conjecture implies that although topological and trivial phases were traditionally considered indistinguishable based on bulk local observables, they can, in fact, be distinguished through their bulk entanglement spectrum. More broadly, the Li-Haldane conjecture was originally proposed to investigate the topological properties of fractional quantum Hall states. It was later generalized to both non-interacting and interacting gapped SPT phases [60, 61, 63–65, 73], and more recently, to interacting bosonic symmetry-enriched QCPs [33, 50].

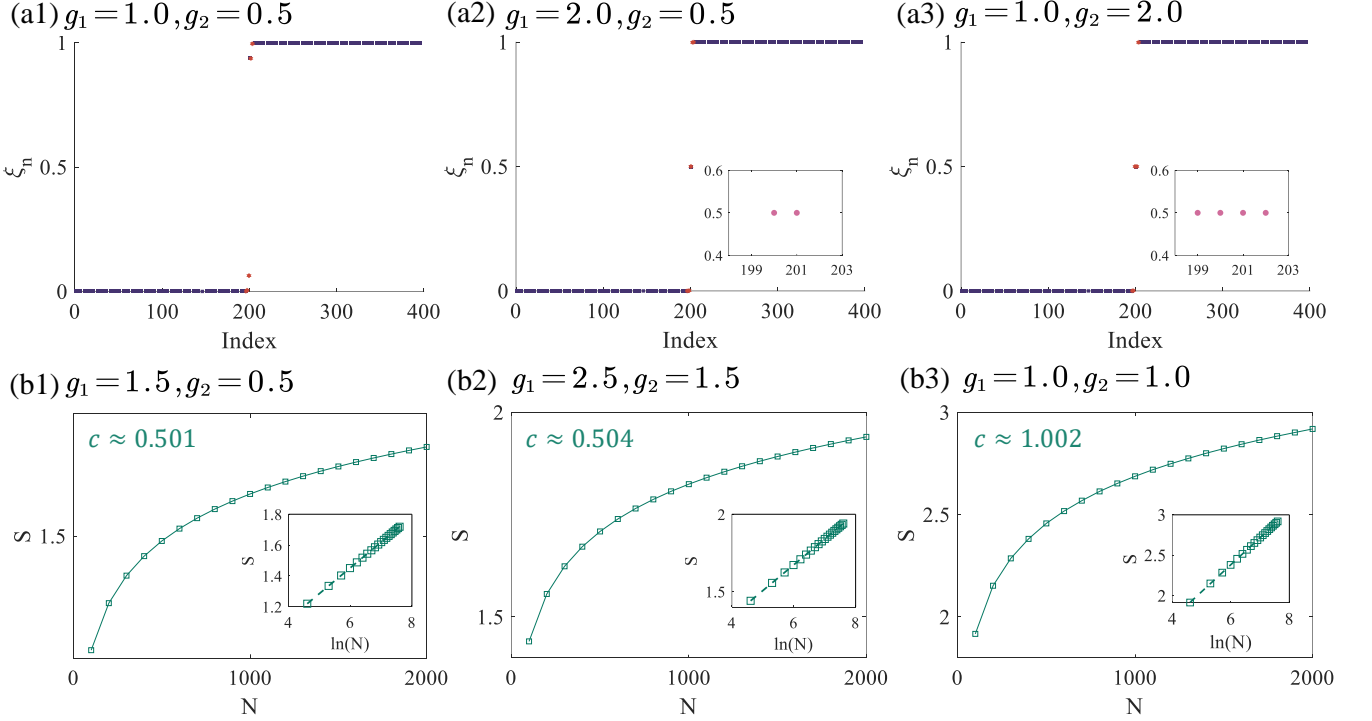


FIG. 3. (Color Online) The entanglement spectrum $\{\xi_n\}$ under periodic boundary conditions at representative points within the trivial (a1), $\omega = 1$ TSC (a2), and $\omega = 2$ TSC (a3) phases is shown. The insets of (a2) and (a3) display dangling degenerate edge modes, revealing the topological degeneracy in the entanglement spectrum, consistent with the Li-Haldane conjecture. Simulations are performed with a system size of $N = 200$. The insets show the degenerate edge modes by zooming in on isolated points in the spectrum. At selected points along the three conformal critical lines, we examine the scaling of the half-chain entanglement entropy S at the trivial (b1) and topologically nontrivial (b2) Majorana critical points, as well as at the Dirac universality class critical point (b3). The inset shows a log-log plot of S , capturing the central charge of the underlying conformal critical point according to the relation $S(N) \sim \frac{c}{6} \ln N + \text{const}$. The system size is chosen as $N = 100, 200, \dots, 2000$.

This work aims to employ quantum entanglement diagnostics to probe topological degeneracy in the Majorana α chain described by Eq. (1). For completeness, we first focus on fermionic gapped topological phases, which have been extensively studied in the literature [3]. We select one representative point from each region of the phase diagram and compute the bulk entanglement spectrum $\{\xi_n\}$, as shown in Fig. 3 (a1-a3). For $g_1 = 1.0, g_2 = 0.5$, the bulk entanglement spectrum does not exhibit any degeneracy (Fig. 3(a1)), indicating that this region corresponds to a topologically trivial phase. In contrast, for $g_1 = 2.0, g_2 = 0.5$ and $g_1 = 1.0, g_2 = 2.0$, the bulk entanglement spectrum exhibits two-fold and four-fold degeneracy, respectively, implying that these regions correspond to topologically nontrivial phases with winding numbers $\omega = 1$ and $\omega = 2$ (see the insets of Fig. 3(a2-a3)). Furthermore, as confirmed in Appendix B, these topological edge modes are also reflected in the energy spectrum under open boundary conditions, providing numerical verification of the Li-Haldane bulk-boundary correspondence in fermionic SPT states. Additional numerical evidence at other points in the phase diagram can be found in Appendix D.

D. Entanglement entropy and spectrum in fermionic symmetry-enriched QCPs

1. Entanglement entropy

After exploring the entanglement properties of all quantum phases, we now shift our focus to the more intriguing QCPs between these phases from the perspective of entanglement. To explore the universality along the transition lines, we first examine the half-chain entanglement entropy S at three critical points in the phase diagram. As shown in Fig. 3 (b1-b3), we select three representative points along the transition lines and compute the scaling behavior of S for different system sizes N . For $g_1 = 1.5, g_2 = 0.5$ and $g_1 = 2.5, g_2 = 1.5$, which correspond to transition points between a TSC with winding number $\omega = 1$ and a trivial phase (Fig. 3 (b1)) or between a TSC with $\omega = 1$ and another with $\omega = 2$ (Fig. 3 (b2)), respectively, the numerical results unambiguously demonstrate that the entanglement entropy at these critical points follows a logarithmic scaling (see the insets of Fig. 3 (b1-b3)). This confirms that the transitions are described by a conformally invariant field theory with central charge $c = 1/2$, placing them in the Majorana universality class [71, 72]. Conversely,

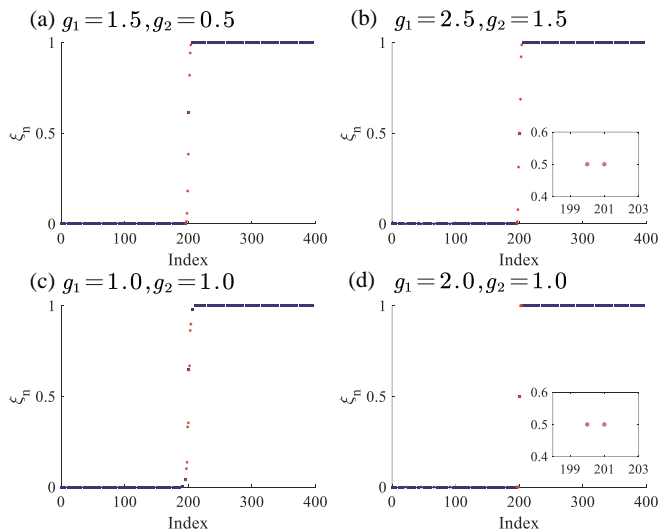


FIG. 4. (Color Online) The entanglement spectrum at four different critical points is shown. (a) The conformal critical point between the trivial and $\omega = 1$ TSC phases. (b) The conformal critical point between the $\omega = 1$ and $\omega = 2$ TSC phases. (c) The conformal critical point between the trivial and $\omega = 2$ TSC phases. (d) The nonconformal multicritical point at the intersection of the three critical lines. The insets show the degenerate edge modes by zooming in on isolated points in the spectrum. Simulations are performed with a system size of $N = 200$.

for the transition point at $g_1 = 1.0, g_2 = 1.0$, which separates the trivial phase from a TSC phase with winding number $\omega = 2$ (Fig. 3 (b3)), the entanglement entropy at criticality also follows a logarithmic scaling but with a central charge of $c = 1$, indicating that this transition belongs to the Dirac universality class [35, 57]. Additional numerical evidence supporting these findings for other points along the transition lines is provided in Appendix C. Interestingly, for quantum critical lines that are topologically distinct—such as the two $c = 1/2$ Majorana critical lines mentioned above—entanglement entropy alone fails to distinguish the underlying nontrivial topology. This limitation can be overcome by analyzing the bulk entanglement spectrum, which we discuss in the next subsection. Finally, the entanglement entropy at the Lifshitz multicritical point ($g_1 = 2, g_2 = 1$) exhibits anomalous scaling behavior due to the absence of conformal invariance, which has recently attracted great attention [89, 90].

2. Entanglement spectrum

To reveal the nontrivial topology along the quantum critical lines, we examine the bulk entanglement spectrum to identify possible topological degeneracies based on the Li-Haldane bulk-boundary correspondence. Specifically, we first focus on the entanglement spectrum at the transition point between trivial and TSC phases with winding numbers $\omega = 1$ and 2, respectively. As illustrated in Fig. 4(a) and (c), we observe that the bulk entanglement spectrum does not exhibit any degeneracy, which is consistent with the features

of the energy spectrum under open boundary conditions, as shown in Appendix B. These results imply that both critical points between trivial and TSC phases with different winding numbers belong to a topologically trivial universality class, in agreement with previous theoretical arguments [35, 57]. Conversely, the entanglement spectra at the remaining critical and multicritical points, shown in Fig. 4(b) and (d), exhibit nontrivial topological degeneracy. More precisely, our numerical results unambiguously demonstrate that the entanglement spectrum of the conformal critical point between TSC phases with winding numbers $\omega = 1$ and 2—and, more surprisingly, the nonconformal Lifshitz multicritical point—both display two-fold topological degeneracy in the bulk entanglement spectrum. This degeneracy is also consistent with the energy spectrum under open boundary conditions, further supporting the predictions of the Li-Haldane bulk-boundary correspondence. Additional numerical evidence for the entanglement spectra at other points along the critical line can be found in Appendix D. Consequently, we demonstrate that the bulk entanglement spectrum serves as an effective diagnostic tool for distinguishing fermionic symmetry-enriched QCPs in non-interacting systems.

Finally, we would like to make one additional remark: as in the case of gapped SPT phases, the classification of bosonic and fermionic SPT phases generally follows distinct theoretical frameworks [4, 10, 11, 91–93]. Therefore, it is essential to investigate the topological properties of bosonic and fermionic symmetry-enriched QCPs separately. Our previous work [33] focused on the entanglement spectrum of bosonic symmetry-enriched QCPs in one-dimensional, strongly interacting quantum spin chains. Extending the notion of gapless topology to higher-dimensional, strongly interacting systems presents considerable analytical and numerical challenges due to the lack of well-established theoretical frameworks and efficient many-body computational algorithm. In contrast, free fermion critical systems do not suffer from these limitations, making them a promising platform for studying higher-dimensional symmetry-enriched QCPs. In Appendix E, we present additional numerical simulations and a brief discussion of two-dimensional fermionic symmetry-enriched QCPs from the entanglement perspective. A more systematic study of higher-dimensional symmetry-enriched QCPs, particularly in interacting systems, is considerably more involved and beyond the scope of the present work, but we regard it as an important direction for future research.

IV. CONCLUSION AND OUTLOOK

To summarize, using the critical Majorana α -chain with time-reversal and particle-hole symmetries as an illustrative example, we have explored quantum entanglement properties and established a bulk-boundary correspondence reflected in the bulk entanglement spectrum for both gapped and gapless fermionic topological states. Specifically, employing entanglement entropy and spectrum as diagnostic tools, we obtain a global phase diagram for the Hamiltonian, which interpolates between different fixed-point Hamiltonians for H_0, H_1 , and

H_2 . The competition between tuning parameters gives rise to trivial and topologically nontrivial gapped phases with winding numbers $\omega = 1$ and 2 , as confirmed numerically through the topological degeneracy in the bulk entanglement spectrum, in accordance with the Li-Haldane conjecture. More importantly, the transition lines in the phase diagram can be analytically determined due to the solvability of the free fermion model. By analyzing the scaling of entanglement entropy, we find that both transitions between the $\omega = 1$ TSC phase and either the trivial or $\omega = 2$ TSC phase belong to the Majorana universality class with central charge $c = 1/2$, whereas the transition between the trivial and $\omega = 2$ TSC phase belongs to the Dirac universality class with $c = 1$. Furthermore, the topological distinctions between these three critical lines can be revealed through the nontrivial degeneracy of the bulk entanglement spectrum, providing an effective diagnostic for probing nontrivial topology based solely on bulk quantities and generalizing the Li-Haldane bulk-boundary correspondence to fermionic symmetry-enriched QCPs. Additionally, we examine the topological properties at the intersection of the three

transition lines and identify a topological Lifshitz multicritical point characterized by two-fold degeneracy in the entanglement spectrum. Future directions of interest include extending the bulk-boundary correspondence in entanglement spectra to higher dimensions and developing a comprehensive theory of quantum entanglement in symmetry-enriched QCPs, at least for free fermion systems. Our work sheds new light on the underlying mechanisms of quantum entanglement in gapless topological phases of matter.

ACKNOWLEDGMENTS

X.-J. Yu thank Shao-Kai Jian and Sheng Yang for collaboration on related projects. We thank Zhi-Kang Lin for helpful discussions. X.-J. Yu was supported by the National Natural Science Foundation of China (Grant No.12405034) and a start-up grant from Fuzhou University. H.Q. Lin acknowledges financial support from NSFC12088101 and MOST 2022YFA1402701.

-
- [1] X.-L. Qi and S.-C. Zhang, Topological insulators and superconductors, *Rev. Mod. Phys.* **83**, 1057 (2011).
 - [2] M. Z. Hasan and C. L. Kane, Colloquium: Topological insulators, *Rev. Mod. Phys.* **82**, 3045 (2010).
 - [3] X.-G. Wen, Colloquium: Zoo of quantum-topological phases of matter, *Rev. Mod. Phys.* **89**, 041004 (2017).
 - [4] T. Senthil, Symmetry-protected topological phases of quantum matter, *Annu. Rev. Condens. Matter Phys.* **6**, 299 (2015).
 - [5] C. L. Kane and E. J. Mele, Z_2 topological order and the quantum spin hall effect, *Phys. Rev. Lett.* **95**, 146802 (2005).
 - [6] C. L. Kane and E. J. Mele, Quantum spin hall effect in graphene, *Phys. Rev. Lett.* **95**, 226801 (2005).
 - [7] B. A. Bernevig, T. L. Hughes, and S.-C. Zhang, Quantum spin hall effect and topological phase transition in hgte quantum wells, *Science* **314**, 1757 (2006), <https://www.science.org/doi/pdf/10.1126/science.1133734>.
 - [8] M. König, S. Wiedmann, C. Brüne, A. Roth, H. Buhmann, L. W. Molenkamp, X.-L. Qi, and S.-C. Zhang, Quantum spin hall insulator state in hgte quantum wells, *Science* **318**, 766 (2007), <https://www.science.org/doi/pdf/10.1126/science.1148047>.
 - [9] Z.-C. Gu and X.-G. Wen, Tensor-entanglement-filtering renormalization approach and symmetry-protected topological order, *Phys. Rev. B* **80**, 155131 (2009).
 - [10] X. Chen, Z.-C. Gu, Z.-X. Liu, and X.-G. Wen, Symmetry protected topological orders and the group cohomology of their symmetry group, *Phys. Rev. B* **87**, 155114 (2013).
 - [11] X. Chen, Z.-C. Gu, Z.-X. Liu, and X.-G. Wen, Symmetry-protected topological orders in interacting bosonic systems, *Science* **338**, 1604 (2012), <https://www.science.org/doi/pdf/10.1126/science.1227224>.
 - [12] F. Pollmann and A. M. Turner, Detection of symmetry-protected topological phases in one dimension, *Phys. Rev. B* **86**, 125441 (2012).
 - [13] X. G. WEN, Topological orders in rigid states, *International Journal of Modern Physics B* **04**, 239 (1990), <https://doi.org/10.1142/S0217979290000139>.
 - [14] X.-G. Wen, Topological orders and edge excitations in fractional quantum hall states, *Advances in Physics* **44**, 405 (1995).
 - [15] Y. Zhou, K. Kanoda, and T.-K. Ng, Quantum spin liquid states, *Rev. Mod. Phys.* **89**, 025003 (2017).
 - [16] L. Savary and L. Balents, Quantum spin liquids: a review, *Reports on Progress in Physics* **80**, 016502 (2016).
 - [17] X.-G. Wen, Choreographed entanglement dances: Topological states of quantum matter, *Science* **363**, eaal3099 (2019), <https://www.science.org/doi/pdf/10.1126/science.aal3099>.
 - [18] C. Broholm, R. J. Cava, S. A. Kivelson, D. G. Nocera, M. R. Norman, and T. Senthil, Quantum spin liquids, *Science* **367**, eaay0668 (2020), <https://www.science.org/doi/pdf/10.1126/science.aay0668>.
 - [19] M. Cheng and H.-H. Tu, Majorana edge states in interacting two-chain ladders of fermions, *Phys. Rev. B* **84**, 094503 (2011).
 - [20] L. Fidkowski, R. M. Lutchyn, C. Nayak, and M. P. A. Fisher, Majorana zero modes in one-dimensional quantum wires without long-ranged superconducting order, *Phys. Rev. B* **84**, 195436 (2011).
 - [21] J. P. Kestner, B. Wang, J. D. Sau, and S. Das Sarma, Prediction of a gapless topological haldane liquid phase in a one-dimensional cold polar molecular lattice, *Phys. Rev. B* **83**, 174409 (2011).
 - [22] A. Keselman and E. Berg, Gapless symmetry-protected topological phase of fermions in one dimension, *Phys. Rev. B* **91**, 235309 (2015).
 - [23] J. Ruhman and E. Altman, Topological degeneracy and pairing in a one-dimensional gas of spinless fermions, *Phys. Rev. B* **96**, 085133 (2017).
 - [24] D. E. Parker, T. Scaffidi, and R. Vasseur, Topological luttinger liquids from decorated domain walls, *Phys. Rev. B* **97**, 165114 (2018).
 - [25] H.-C. Jiang, Z.-X. Li, A. Seidel, and D.-H. Lee, Symmetry protected topological luttinger liquids and the phase transition between them, *Science Bulletin* **63**, 753 (2018).
 - [26] A. Keselman, E. Berg, and P. Azaria, From one-dimensional charge conserving superconductors to the gapless haldane phase, *Phys. Rev. B* **98**, 214501 (2018).

- [27] T. Scaffidi, D. E. Parker, and R. Vasseur, Gapless symmetry-protected topological order, *Phys. Rev. X* **7**, 041048 (2017).
- [28] R. Thorngren, A. Vishwanath, and R. Verresen, Intrinsically gapless topological phases, *Phys. Rev. B* **104**, 075132 (2021).
- [29] R. Verresen, R. Thorngren, N. G. Jones, and F. Pollmann, Gapless topological phases and symmetry-enriched quantum criticality, *Phys. Rev. X* **11**, 041059 (2021).
- [30] R. Verresen, Topology and edge states survive quantum criticality between topological insulators, [arXiv:2003.05453](#) (2020).
- [31] C. M. Duque, H.-Y. Hu, Y.-Z. You, V. Khemani, R. Verresen, and R. Vasseur, Topological and symmetry-enriched random quantum critical points, *Phys. Rev. B* **103**, L100207 (2021).
- [32] X.-J. Yu, R.-Z. Huang, H.-H. Song, L. Xu, C. Ding, and L. Zhang, Conformal boundary conditions of symmetry-enriched quantum critical spin chains, *Phys. Rev. Lett.* **129**, 210601 (2022).
- [33] X.-J. Yu, S. Yang, H.-Q. Lin, and S.-K. Jian, Universal entanglement spectrum in one-dimensional gapless symmetry protected topological states, *Phys. Rev. Lett.* **133**, 026601 (2024).
- [34] D. E. Parker, R. Vasseur, and T. Scaffidi, Topologically protected long edge coherence times in symmetry-broken phases, *Phys. Rev. Lett.* **122**, 240605 (2019).
- [35] X.-J. Yu and W.-L. Li, Fidelity susceptibility at the lifshitz transition between the noninteracting topologically distinct quantum critical points, *Phys. Rev. B* **110**, 045119 (2024).
- [36] S. Yang, H.-Q. Lin, and X.-J. Yu, Gapless topological behaviors in a long-range quantum spin chain, *Communications Physics* **8**, 27 (2025).
- [37] W.-H. Zhong, W.-L. Li, Y.-C. Chen, and X.-J. Yu, Topological edge modes and phase transitions in a critical fermionic chain with long-range interactions, *Phys. Rev. A* **110**, 022212 (2024).
- [38] U. Borla, R. Verresen, J. Shah, and S. Moroz, Gauging the Kitaev chain, *SciPost Phys.* **10**, 148 (2021).
- [39] A. J. Friedman, B. Ware, R. Vasseur, and A. C. Potter, Topological edge modes without symmetry in quasiperiodically driven spin chains, *Phys. Rev. B* **105**, 115117 (2022).
- [40] L. Li, M. Oshikawa, and Y. Zheng, Intrinsically/purely gapless-spt from non-invertible duality transformations (2023), [arXiv:2307.04788](#) (2023).
- [41] S.-J. Huang and M. Cheng, Topological holography, quantum criticality, and boundary states, [arXiv:2310.16878](#) (2023).
- [42] R. Wen and A. C. Potter, Bulk-boundary correspondence for intrinsically gapless symmetry-protected topological phases from group cohomology, *Phys. Rev. B* **107**, 245127 (2023).
- [43] M. Jangjan, L. E. F. Foa Torres, and M. V. Hosseini, Floquet topological phase transitions in a periodically quenched dimer, *Phys. Rev. B* **106**, 224306 (2022).
- [44] M. Jangjan and M. V. Hosseini, Topological properties of subsystem-symmetry-protected edge states in an extended quasi-one-dimensional dimerized lattice, *Phys. Rev. B* **106**, 205111 (2022).
- [45] R. Wen and A. C. Potter, Classification of 1+1d gapless symmetry protected phases via topological holography, [arXiv:2311.00050](#) (2023).
- [46] R. Wen, String condensation and topological holography for 2+1d gapless spt, [arXiv:2408.05801](#) (2024).
- [47] L. Li, M. Oshikawa, and Y. Zheng, Decorated defect construction of gapless-SPT states, *SciPost Phys.* **17**, 013 (2024).
- [48] S.-J. Huang, Fermionic quantum criticality through the lens of topological holography, [arXiv:2405.09611](#) (2024).
- [49] L. Su and M. Zeng, Gapless symmetry-protected topological phases and generalized deconfined critical points from gauging a finite subgroup, *Phys. Rev. B* **109**, 245108 (2024).
- [50] H.-L. Zhang, H.-Z. Li, S. Yang, and X.-J. Yu, Quantum phase transition and critical behavior between the gapless topological phases, *Phys. Rev. A* **109**, 062226 (2024).
- [51] T. Ando, S. Ryu, and M. Watanabe, Gauge theory and mixed state criticality, [arXiv:2411.04360](#) (2024).
- [52] L. Zhou, J. Gong, and X.-J. Yu, Topological edge states at floquet quantum criticality, *Communications Physics* **8**, 214 (2025).
- [53] L. Li, R.-Z. Huang, and W. Cao, Noninvertible symmetry-enriched quantum critical point, [arXiv:2411.19034](#) (2024).
- [54] X.-J. Yu, S. Yang, S. Liu, H.-Q. Lin, and S.-K. Jian, Gapless symmetry-protected topological states in measurement-only circuits (2025), [arXiv:2501.03851](#) [cond-mat.str-el].
- [55] Z. Tan, K. Wang, S. Yang, F. Shen, F. Jin, X. Zhu, Y. Ji, S. Xu, J. Chen, Y. Wu, C. Zhang, Y. Gao, N. Wang, Y. Zou, A. Zhang, T. Li, Z. Bao, Z. Zhu, J. Zhong, Z. Cui, Y. Han, Y. He, H. Wang, J. Yang, Y. Wang, J. Shen, G. Liu, Z. Song, J. Deng, H. Dong, P. Zhang, S.-K. Jian, H. Li, Z. Wang, Q. Guo, C. Song, X.-J. Yu, H. Wang, H.-Q. Lin, and F. Wu, Exploring nontrivial topology at quantum criticality in a superconducting processor (2025), [arXiv:2501.04679](#) [quant-ph].
- [56] S. Yang, F. Xu, D.-C. Lu, Y.-Z. You, H.-Q. Lin, and X.-J. Yu, Deconfined criticality as intrinsically gapless topological state in one dimension (2025), [arXiv:2503.01198](#) [cond-mat.str-el].
- [57] R. Verresen, N. G. Jones, and F. Pollmann, Topology and edge modes in quantum critical chains, *Phys. Rev. Lett.* **120**, 057001 (2018).
- [58] N. Laflorencie, Quantum entanglement in condensed matter systems, *Physics Reports* **646**, 1 (2016), quantum entanglement in condensed matter systems.
- [59] H. Li and F. D. M. Haldane, Entanglement spectrum as a generalization of entanglement entropy: Identification of topological order in non-abelian fractional quantum hall effect states, *Phys. Rev. Lett.* **101**, 010504 (2008).
- [60] A. M. Turner, F. Pollmann, and E. Berg, Topological phases of one-dimensional fermions: An entanglement point of view, *Phys. Rev. B* **83**, 075102 (2011).
- [61] F. Pollmann, A. M. Turner, E. Berg, and M. Oshikawa, Entanglement spectrum of a topological phase in one dimension, *Phys. Rev. B* **81**, 064439 (2010).
- [62] S. V. Isakov, M. B. Hastings, and R. G. Melko, Topological entanglement entropy of a bose-hubbard spin liquid, *Nature Physics* **7**, 772 (2011).
- [63] X.-L. Qi, H. Katsura, and A. W. W. Ludwig, General relationship between the entanglement spectrum and the edge state spectrum of topological quantum states, *Phys. Rev. Lett.* **108**, 196402 (2012).
- [64] T. H. Hsieh and L. Fu, Bulk entanglement spectrum reveals quantum criticality within a topological state, *Phys. Rev. Lett.* **113**, 106801 (2014).
- [65] G. Y. Cho, K. Shiozaki, S. Ryu, and A. W. W. Ludwig, Relationship between symmetry protected topological phases and boundary conformal field theories via the entanglement spectrum, *Journal of Physics A: Mathematical and Theoretical* **50**, 304002 (2017).
- [66] A. Chandran, V. Khemani, and S. L. Sondhi, How universal is the entanglement spectrum?, *Phys. Rev. Lett.* **113**, 060501 (2014).
- [67] H. Yao and X.-L. Qi, Entanglement entropy and entanglement spectrum of the kitaev model, *Phys. Rev. Lett.* **105**, 080501 (2010).
- [68] M. K. Joshi, C. Kokail, R. van Bijnen, F. Kranzl, T. V. Zache, R. Blatt, C. F. Roos, and P. Zoller, Exploring large-scale entanglement in quantum simulation, *Nature* **624**, 539 (2023).

- [69] T. V. Zache, C. Kokail, B. Sundar, and P. Zoller, Entanglement spectroscopy and probing the li-haldane conjecture in topological quantum matter, *Quantum* **6**, 702 (2022).
- [70] C. Kokail, R. van Bijnen, A. Elben, B. Vermersch, and P. Zoller, Entanglement hamiltonian tomography in quantum simulation, *Nature Physics* **17**, 936 (2021).
- [71] P. Francesco, P. Mathieu, and D. Sénéchal, *Conformal field theory* (Springer Science & Business Media, 2012).
- [72] P. Ginsparg, *Applied conformal field theory* (1988), [arXiv:hep-th/9108028 \[hep-th\]](#).
- [73] L. Fidkowski, Entanglement spectrum of topological insulators and superconductors, *Phys. Rev. Lett.* **104**, 130502 (2010).
- [74] R. Verresen, R. Moessner, and F. Pollmann, One-dimensional symmetry protected topological phases and their transitions, *Phys. Rev. B* **96**, 165124 (2017).
- [75] W. Choi, M. Knap, and F. Pollmann, Finite-temperature entanglement negativity of fermionic symmetry-protected topological phases and quantum critical points in one dimension, *Physical Review B* **109**, 10.1103/physrevb.109.115132 (2024).
- [76] A. Altland and M. R. Zirnbauer, Nonstandard symmetry classes in mesoscopic normal-superconducting hybrid structures, *Phys. Rev. B* **55**, 1142 (1997).
- [77] W. Son, L. Amico, R. Fazio, A. Hamma, S. Pascazio, and V. Vedral, Quantum phase transition between cluster and antiferromagnetic states, *Europhysics Letters* **95**, 50001 (2011).
- [78] P. Smacchia, L. Amico, P. Facchi, R. Fazio, G. Florio, S. Pascazio, and V. Vedral, Statistical mechanics of the cluster ising model, *Phys. Rev. A* **84**, 022304 (2011).
- [79] Z.-X. Guo, X.-J. Yu, X.-D. Hu, and Z. Li, Emergent phase transitions in a cluster ising model with dissipation, *Phys. Rev. A* **105**, 053311 (2022).
- [80] W.-L. Li, Y.-A. Chen, Z.-X. Guo, X.-J. Yu, and Z. Li, Global phase diagram of the cluster-xy spin chain with dissipation, *Phys. Rev. A* **111**, 013316 (2025).
- [81] G. Vidal, J. I. Latorre, E. Rico, and A. Kitaev, Entanglement in quantum critical phenomena, *Phys. Rev. Lett.* **90**, 227902 (2003).
- [82] I. Peschel and V. Eisler, Reduced density matrices and entanglement entropy in free lattice models, *Journal of Physics A: Mathematical and Theoretical* **42**, 504003 (2009).
- [83] L. Zhou, Entanglement spectrum and entropy in floquet topological matter, *Phys. Rev. Res.* **4**, 043164 (2022).
- [84] I. Peschel, Calculation of reduced density matrices from correlation functions, *Journal of Physics A: Mathematical and General* **36**, L205 (2003), [arXiv:cond-mat/0212631](#).
- [85] S.-A. Cheong and C. L. Henley, Many-body density matrices for free fermions (2003), [arXiv:cond-mat/0206196](#).
- [86] P.-Y. Chang, J.-S. You, X. Wen, and S. Ryu, Entanglement spectrum and entropy in topological non-hermitian systems and nonunitary conformal field theory, *Physical Review Research* **2**, 033069 (2020).
- [87] B.-T. Ye, L.-Z. Mu, and H. Fan, Entanglement spectrum of suschrieffer-heeger-hubbard model, *Physical Review B* **94**, 165167 (2016), [arXiv:1602.00488](#).
- [88] N. G. Jones and R. Verresen, Asymptotic correlations in gapped and critical topological phases of 1d quantum systems, *Journal of Statistical Physics* **175**, 1164 (2019).
- [89] K. Wang and T. A. Sedrakyan, Universal finite-size amplitude and anomalous entanglement entropy of $z = 2$ quantum Lifshitz criticalities in topological chains, *SciPost Phys.* **12**, 134 (2022).
- [90] K. Wang, Quantum $z = 2$ lifshitz criticality in one-dimensional interacting fermion systems, *Phys. Rev. B* **108**, L081112 (2023).
- [91] Z. Bi, A. Rasmussen, K. Slagle, and C. Xu, Classification and description of bosonic symmetry protected topological phases with semiclassical nonlinear sigma models, *Phys. Rev. B* **91**, 134404 (2015).
- [92] T. Lan, L. Kong, and X.-G. Wen, Classification of (2+1)-dimensional topological order and symmetry-protected topological order for bosonic and fermionic systems with on-site symmetries, *Phys. Rev. B* **95**, 235140 (2017).
- [93] M. Cheng, Z. Bi, Y.-Z. You, and Z.-C. Gu, Classification of symmetry-protected phases for interacting fermions in two dimensions, *Phys. Rev. B* **97**, 205109 (2018).

Appendix A: EXACT SOLUTION OF MAJORANA α CHAIN

In this section, we provide a detailed analytical solution for the Hamiltonian $H = H_0 - g_1 H_1 + g_2 H_2$. We begin by substituting the relations $\gamma_n = c_n^\dagger + c_n$ and $\tilde{\gamma}_n = i(c_n^\dagger - c_n)$ into the complex fermion c and c^\dagger , yielding

$$H = \sum_n \left[(1 - 2c_n^\dagger c_n) + g_1 (c_n^\dagger c_{n+1} + c_n^\dagger c_{n+1}^\dagger + h.c.) - g_2 (c_n^\dagger c_{n+2} + c_n^\dagger c_{n+2}^\dagger + h.c.) \right], \quad (\text{A1})$$

here $h.c.$ means hermitian conjugate. Then we can derive further result by using Fourier transformation $c_n = \frac{1}{\sqrt{N}} \sum_k e^{-ikn} c_k$, where $k = \pm \frac{(2n-1)\pi}{2}$, $n = 1, 2, \dots, N/2$. Thus the Hamiltonian H in k -space is

$$H = \sum_k \left[i y_k (c_k c_{-k} + c_k^\dagger c_{-k}^\dagger) + z_k (c_k^\dagger c_k + c_{-k}^\dagger c_{-k}) \right], \quad (\text{A2})$$

here, $y_k = g_1 \sin k - g_2 \sin 2k$, and $z_k = g_1 \cos k - g_2 \cos 2k - 1$. To diagonalize the Hamiltonian, we introduce the Bogoliubov transformation:

$$a_k = \cos\left(\frac{\theta_k}{2}\right) c_k - i \sin\left(\frac{\theta_k}{2}\right) c_{-k}^\dagger \quad (\text{A3})$$

$$a_k^\dagger = \cos\left(\frac{\theta_k}{2}\right) c_k^\dagger + i \sin\left(\frac{\theta_k}{2}\right) c_{-k}, \quad (\text{A4})$$

with $\tan \theta_k = -\frac{y_k}{z_k}$. The Hamiltonian can be diagonalized as

$$H = \sum_{k>0} \varepsilon_k \left(a_k^\dagger a_k - \frac{1}{2} \right), \quad (\text{A5})$$

where the quasiparticle dispersion is given by $\varepsilon_k = 4\sqrt{y_k^2 + z_k^2}$. A phase transition occurs when the energy gap closes, i.e., when $\varepsilon_k = 0$, which requires both $y_k = 0$ and $z_k = 0$. At these gapless points, low-energy excitations emerge, leading to singularities in the free energy and other thermodynamic quantities. Therefore, the condition $y_k = z_k = 0$ marks the presence of a gapless excitation, indicating a quantum phase transition.

Moreover, the phase diagram exhibits three quantum phases and the phase transitions between them, as discussed in Sec. II of the main text. We now derive the exact expression for the phase boundary lines in the phase diagram in detail.

We express the equations $y_k = z_k = 0$ as

$$g_1 \sin k - g_2 \sin 2k = \sin k (g_1 - 2g_2 \cos k) = 0, \quad (\text{A6})$$

and

$$g_1 \cos k - g_2 \cos 2k = 1. \quad (\text{A7})$$

From Eq. (A6), there are two possible solutions: $k = 0$ and $\cos k = g_1/(2g_2)$. First, substituting $k = 0$ into Eq. (A7), we immediately obtain $g_1 = g_2 + 1$. This result corresponds to the black and blue dashed lines in Fig. 2. On the other hand, substituting $\cos k = g_1/(2g_2)$ into Eq. (A7) and imposing the constraint $0 < \cos k < 1$, we find that $0 < g_1 < 2$ and $g_2 = 1$. This result corresponds to the white dashed line in Fig. 2. Additionally, there is a critical point at $(g_1, g_2) = (2, 1)$, where the conditions $g_1 = g_2 + 1$ and $g_2 = 1$ are simultaneously satisfied. This point is represented by the purple solid circle in Fig. 2. However, we cannot conclusively determine the universality class of these three phase transition lines or whether they exhibit nontrivial topological properties. Addressing this question is a central focus of our work and underscores the importance of analyzing the quantum entanglement properties of these systems.

Appendix B: NUMERICAL RESULTS FOR ENERGY SPECTRUM UNDER OBCs

In this section, we provide additional numerical data to display the energy spectrum under open boundary conditions (OBCs).

The Hamiltonian can be diagonalized as $H = \sum_{n=1}^N \epsilon_n \eta_n^\dagger \eta_n$ through a canonical Bogoliubov transformation by introducing the fermionic operators η_n and η_n^\dagger ,

$$\eta_n = \sum_i^N (u_{n,i}^* c_i + v_{n,i} c_i^\dagger), \quad \eta_n^\dagger = \sum_i^N (u_{n,i} c_i^\dagger + v_{n,i}^* c_i), \quad (\text{B1})$$

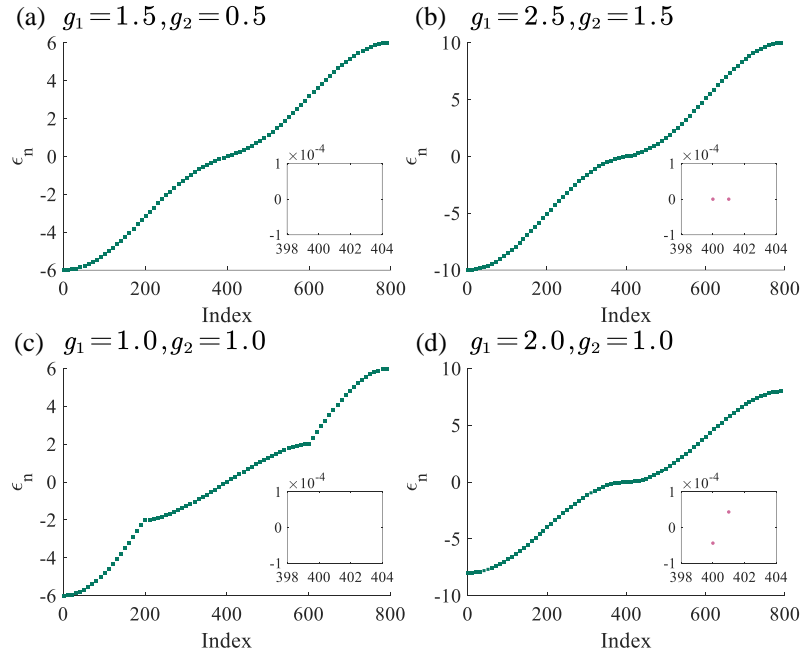


FIG. 5. The open-boundary energy spectrum is shown for the critical points: (a) $(g_1, g_2) = (1.5, 0.5)$, (b) $(g_1, g_2) = (2.5, 1.5)$, (c) $(g_1, g_2) = (1.0, 1.0)$, and (d) $(g_1, g_2) = (2.0, 1.0)$. The insets show the degenerate edge modes by zooming in on isolated points in the spectrum. Simulations are performed for a system size of $N = 400$, displaying data points at intervals of 10 sites, except for the edge states, which are highlighted as purple circle points.

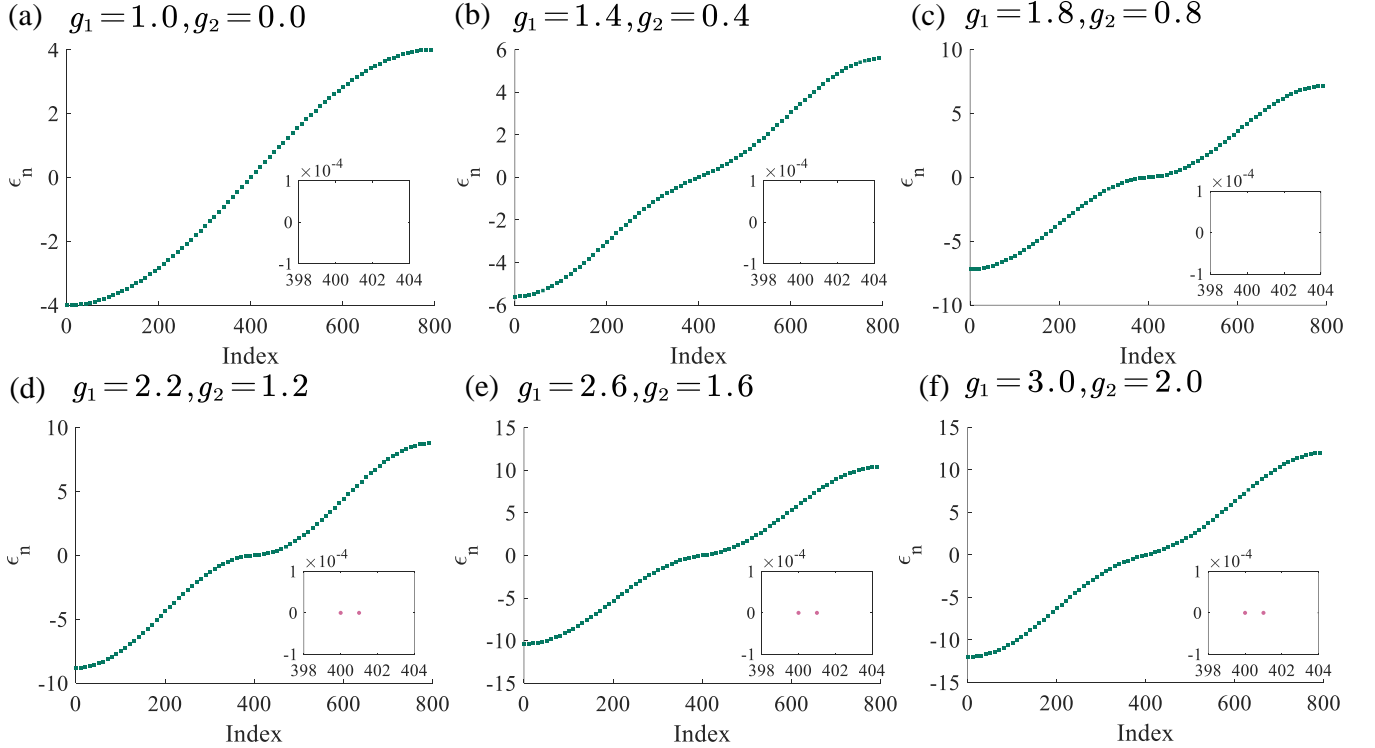


FIG. 6. The open-boundary energy spectrum is shown for additional critical points along three transition lines: (a)(b)(c) along the conformal critical line $(g_1 = g_2 + 1, 0 < g_2 < 1)$, and (d)(e)(f) along the conformal critical line $(g_1 = g_2 + 1, g_2 > 1)$. The insets show the degenerate edge modes by zooming in on isolated points in the spectrum. Simulations are performed for a system size of $N = 400$, displaying data points at intervals of 10 sites, except for the edge states, which are highlighted as purple circle points.

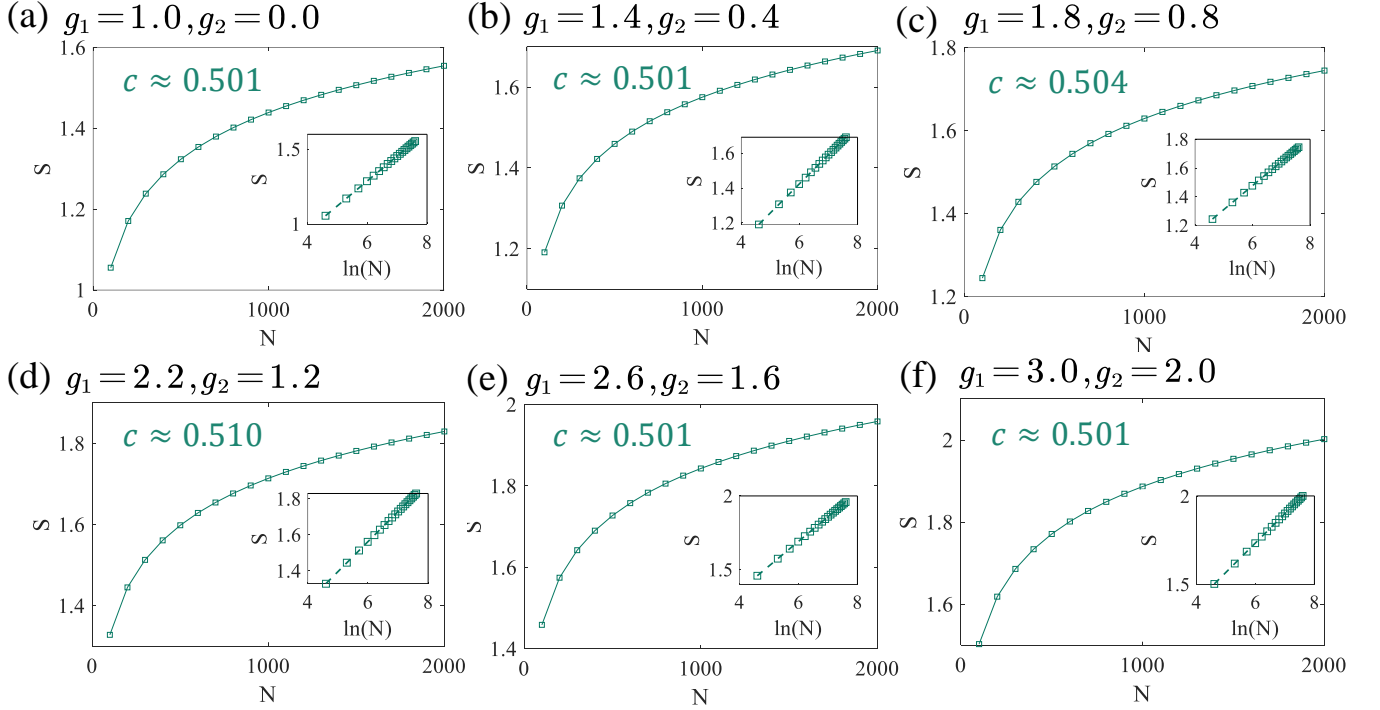


FIG. 7. The entanglement entropy is shown for additional critical points along three transition lines: (a)(b)(c) along the conformal critical line ($g_1 = g_2 + 1$, $0 < g_2 < 1$) and (d)(e)(f) along the conformal critical line ($g_1 = g_2 + 1$, $g_2 > 1$). The insets display the finite-size scaling of the entanglement entropy following the scaling relation $S \sim \frac{c}{3} \ln N + S_0$. The system size is chosen as $N = 100, 200, \dots, 2000$.

where $u_{n,i}$ and $v_{n,i}$ denote the two components of the wave function at site j , n is the energy band index, and ϵ_n represents the eigenstate energy. The Schrödinger equation $H |\Psi_n\rangle = \epsilon_n |\Psi_n\rangle$ can be written as

$$\begin{pmatrix} A & B \\ -B^* & -A^T \end{pmatrix} \begin{pmatrix} u_{n,i} \\ v_{n,i}^* \end{pmatrix} = \epsilon_n \begin{pmatrix} u_{n,i} \\ v_{n,i}^* \end{pmatrix}, \quad (\text{B2})$$

where $A(B)$ is a $N \times N$ symmetric (antisymmetric) matrix, the zero energy state probability distributions can be computed as $|\Psi_{n,i}|^2 = |u_{n,i}|^2 + |v_{n,i}|^2$.

To establish the Li-Haldane bulk-boundary correspondence [59], which states that the low-lying structure of the bulk entanglement spectrum is equivalent to the energy spectrum under open boundary conditions, we select the same parameter points as those used for the entanglement spectrum calculations in the main text: (a) $(g_1, g_2) = (1.5, 0.5)$, (b) $(g_1, g_2) = (2.5, 1.5)$, (c) $(g_1, g_2) = (1.0, 1.0)$, and (d) $(g_1, g_2) = (2.0, 1.0)$. The numerical results for the energy spectrum as a function of the state index are shown in Fig. 5. Comparing these results with Fig. 4 in the main text, we observe that at the critical points lying on the three different conformal critical lines (Fig. 4(a)(b)(c) and Fig. 5(a)(b)(c)), both spectra exhibit the same two-fold topological degeneracy, consistent with the Li-Haldane conjecture, even in fermionic symmetry-enriched QCPs. However, at the nonconformal Lifshitz multicritical point, the Li-Haldane bulk-boundary correspondence appears to break down, as indicated by the absence of exact degeneracy in the open-boundary energy spectrum, despite the presence of double degeneracy in the bulk entanglement spectrum discussed in the main text. Consequently, we termed the multicritical point as topologically nontrivial in the sense that it exhibits nontrivial degeneracy in the bulk energy spectrum. A more detailed and systematic study of the relationship between the energy spectrum and the entanglement spectrum is left for future work.

Additionally, we present numerical results for the energy spectrum under open boundary conditions for additional points along the three transition lines, as shown in Fig. 6. Combining these results with the bulk energy spectrum at shown in Fig. 8, our results unambiguously demonstrate that the three conformal critical lines are topologically distinct and satisfy the Li-Haldane bulk-boundary correspondence.

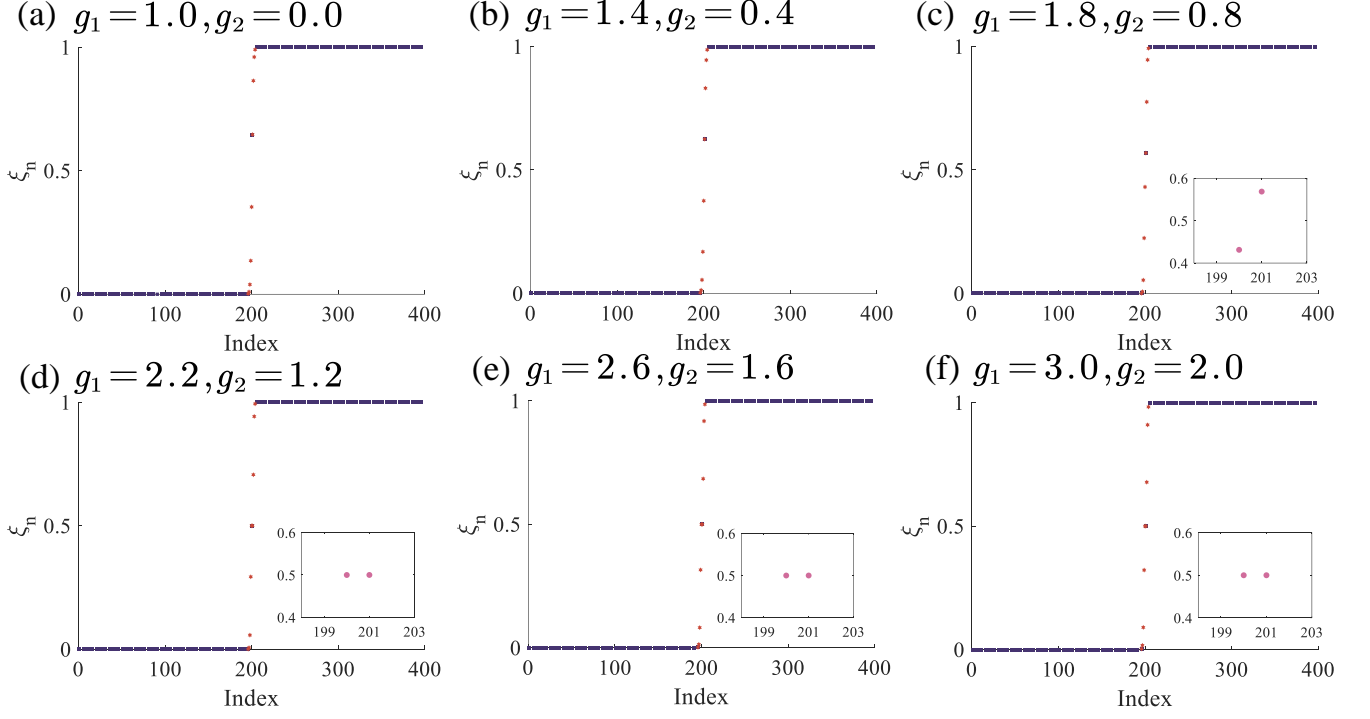


FIG. 8. The bulk entanglement spectrum is shown for additional critical points along three transition lines: (a)(b)(c) along the conformal critical line ($g_1 = g_2 + 1$, $0 < g_2 < 1$) and (d)(e)(f) along the conformal critical line ($g_1 = g_2 + 1$, $g_2 > 1$). The insets show the degenerate edge modes by zooming in on isolated points in the spectrum. Simulations are performed for a system size of $N = 200$.

Appendix C: ADDITIONAL DATA FOR ENTANGLEMENT ENTROPY

In this section, we provide additional numerical data for the half-chain entanglement entropy S . Similar to the analysis in the main text, we present the finite-size scaling of S at additional critical points along the three transition lines in Fig. 7: (a) $(g_1, g_2) = (1.0, 0.0)$, (b) $(g_1, g_2) = (1.4, 0.4)$, and (c) $(g_1, g_2) = (1.8, 0.8)$; (d) $(g_1, g_2) = (2.2, 1.2)$, (e) $(g_1, g_2) = (2.6, 1.6)$, and (f) $(g_1, g_2) = (3.0, 2.0)$. The numerical results confirm that all three critical lines exhibit conformal invariance, as evidenced by the logarithmic scaling of the entanglement entropy. More importantly, the extracted central charge from the scaling relation $S \sim \frac{c}{3} \ln N + S_0$ aligns with the expected Majorana or Dirac universality class, corresponding to $c = 1/2$ or $c = 1$, respectively.

Appendix D: ADDITIONAL DATA FOR ENTANGLEMENT SPECTRUM

In this section, we provide additional numerical data on the bulk entanglement spectrum under periodic boundary conditions. Similar to the main text, the entanglement spectrum is directly related to the eigenvalues $\{\xi_n\}$ of the block correlation function, defined as $G = \mathcal{G}|_A$. Specifically, we numerically compute the entanglement spectrum and present ξ_n as a function of the state index for simplicity. Additional points along the three transition lines are shown in Fig. 8: (a) $(g_1, g_2) = (1.0, 0.0)$, (b) $(g_1, g_2) = (1.4, 0.4)$, (c) $(g_1, g_2) = (1.8, 0.8)$, (d) $(g_1, g_2) = (2.2, 1.2)$, (e) $(g_1, g_2) = (2.6, 1.6)$, and (f) $(g_1, g_2) = (3.0, 2.0)$. The numerical results confirm the emergence of fermionically topologically distinct quantum critical lines in the phase diagram and provide further evidence that the entanglement spectrum serves as an effective diagnostic for detecting nontrivial topology at criticality.

Appendix E: QUANTUM ENTANGLEMENT IN TOPOLOGICALLY DISTINCT CHERN CRITICALITY IN TWO DIMENSION

In this section, we provide additional numerical evidence to demonstrate nontrivial gapless topology in higher dimension can be identified from entanglement point of view. We consider a two dimensional fermionic lattice model for Chern insulator

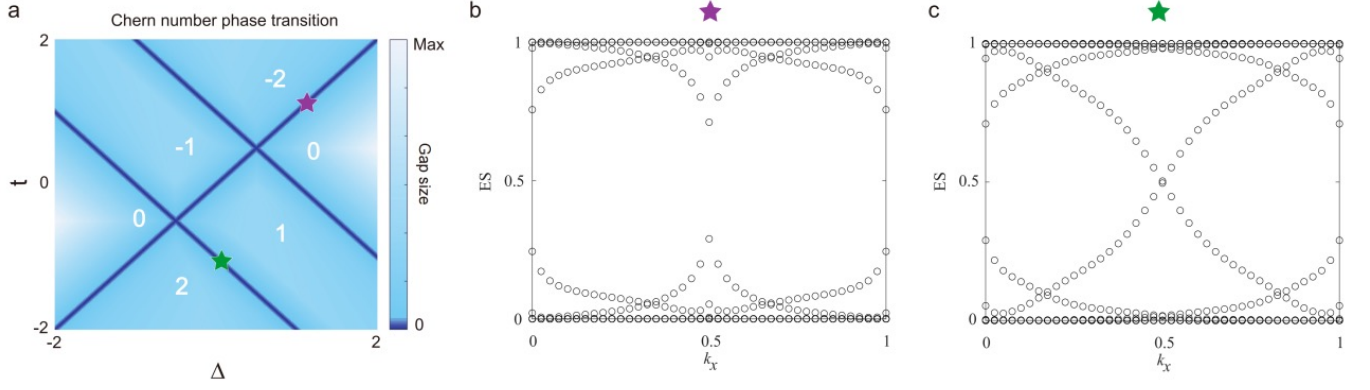


FIG. 9. (a) Phase diagram of a two dimensional fermionic lattice model Eq.(E1) (b) Bulk entanglement spectrum at the critical point between phases with Chern numbers 0 and -2 ($t = 1.0, \Delta = 1.0$), corresponding to the purple star in the panel (a). (c) Bulk entanglement spectrum at the critical point between phases with Chern numbers 1 and 2 ($t = -1.0, \Delta = 0.0$), corresponding to the green star in the panel (a). All simulations are performed on systems with $N = 40 \times 40$ unit cells, with the entanglement computed for a subsystem of 40×10 unit cells.

transition [30], which can be expressed in the momentum space under PBC:

$$H_\alpha = \sum_{\mathbf{k}} \begin{pmatrix} c_{\mathbf{k},A}^\dagger & c_{\mathbf{k},B}^\dagger \end{pmatrix} \mathcal{H}(\mathbf{k}) \begin{pmatrix} c_{\mathbf{k},A} \\ c_{\mathbf{k},B} \end{pmatrix} \quad \text{with } \mathcal{H}(\mathbf{k}) = (\sin(k_x)\sigma_x - \sin(k_y)\sigma_y + (-\Delta - \frac{\cos(k_x)}{2} - \frac{\cos(k_y)}{2} - t \cos(k_x + k_y))\sigma_z, \quad (\text{E1})$$

where t and Δ serve as tuning parameters, with the resulting phase diagram displayed in Fig. 9 (a). We focus on the direct transitions between $C = 0 \leftrightarrow C = -2$ and $C = 1 \leftrightarrow C = 2$ are topologically distinct Dirac cones, respectively. To investigate the topological properties at criticality, we compute bulk entanglement spectrum at two topologically distinct critical points, as shown in Fig. 9 (b) and (c). Specifically, the entanglement spectrum is plotted as a function of k_x , indicating that the system has open boundary conditions along the y -direction and periodic boundary conditions along the x -direction. The entanglement spectrum at the critical point $(t, \Delta) = (-1.0, 0.0)$ unambiguously displays chiral edge states (midgap states in the spectra), which are absent at $(t, \Delta) = (1, 1)$. This contrast not only reinforces the utility of the entanglement spectrum as a diagnostic tool for distinguishing fermionic symmetry-enriched QCPs in higher dimensions but also highlights a promising route for systematically studying higher-dimensional fermionic symmetry-enriched QCPs without resorting to large-scale many-body computations.